Interfacial Phenomena and Heat Transfer, 2 (1): 85–102 (2014)

GRAVITY EFFECT ON EVAPORATION AND INTERFACIAL DEFORMATIONS IN NONISOTHERMAL LIQUID FILM MOVED BY A GAS FLOW IN A MICROGAP

Yu. Kabova,[1,*] V. V. Kuznetsov,[2,3] & O. Kabov[1,4]

[1]*Institute of Thermophysics, SB RAS, 630090, Novosibirsk, pr. Lavrentyev 1, Russia*

[2]*Lavrentyev Institute of Hydrodynamics, SB RAS, 630090, Novosibirsk, pr. Lavrentyev 15, Russia*

[3]*Novosibirsk State University, 630090, Novosibirsk, Pirogova Str., 2, Russia*

[4]*Tomsk Polytechnic University, 634050, Tomsk, Lenin Avenue, 30, Russia*

[*] Address all correspondence to Yu. Kabova, E-mail: kabova@itp.nsc.ru

In the present paper, we investigate evaporating locally heated thin liquid film driven by the action of gas flow in a microgap. A two-sided three-dimensional mathematical model is used. For a deformable gas-liquid interface, convection heat transfer in the liquid and the gas phases as well as temperature dependence of surface tension and liquid viscosity are taken into account. Interaction and balancing of different effects on the evaporation process along the gas-liquid interface takes place. The influences of gravity force, the gas flow rate, and heating intensity on the evaporation rate and gas-liquid interface deformations have been investigated numerically using the developed model. It is shown that evaporation is governed substantially by the gravity and the relation is strongly nonlinear, which could be explained by smoothing of deformations at the gas-liquid interface with gravity changing. The qualitatively different effect of gas velocity on the evaporation rate has been found, depending on the thermal boundary condition on the heated substrate.

KEY WORDS: *evaporation, liquid film, local heat source, thermocapillarity, deformable gas-liquid interface, numerical investigation*

1. INTRODUCTION

Gas-liquid systems with deformable free interfaces moving in microchannels with heat and mass transfer are widely encountered in practice and nature. Cooling of microelectronic equipment (Bar-Cohen et al., 1995, 2012), thermal management systems for space applications (Celata et al., 2008), and microfluidic devices (Squires and Quake, 2005) are just some examples. Because of such widespread applications, liquid film flow with evaporation has gotten considerable attention.

Heat and mass transfer over a vertical falling film was examined numerically and experimentally by Chandra and Savery (1974) where measured temperature and concentration distributions along the gas-liquid interface were used to specify the inhomogeneous boundary conditions required for solving the energy and diffusion equations. Linear stability of liquid film with interfacial phase change was investigated by Spindler (1981); the effect of thickness variation caused by the phase change was taken into account. Heat and mass transfer in the air stream, with negligible effects of liquid film, were considered in Schroppel and Thiele (1983) and Chow and Chung (1983). The effect of finite liquid film on laminar convective heat and mass transfer in a vertical channel, including the transport processes in the gas flow and liquid film was investigated by Yan (1992). The influence of various parameters such as wall heating flux,

2152–5080/14/$35.00

NOMENCLATURE

A	dimensionless number ($g\cos\alpha H_0^2/U^2 l$)	S_0	heating area (m^2)
b	heat transfer coefficient [W/(m$^2\cdot$ K)]	$\mathbf{S}_g$	modified Schmidt number ($\mu_{0g}H_0/D\rho_g$)
c_p	specific heat of the liquid [J/(kg $\cdot$ K)]	t	time (s)
C	mass fraction of moisture in the gas phase	T	temperature (°C)
C	inverse Froude number ($g\sin\alpha H_0/U^2$)	[T]	characteristic scale of the temperature (K)
$C_*(T)$	mass fraction of moisture in the gas phase corresponding to the pressure of the saturated vapor at the temperature T	U	characteristic scale of the liquid velocity, m/s
D	diffusion coefficient (m^2/s)	v	velocity vector
D	modified Prandtl number ($c_p\mu_0 H_0/l\kappa$)	u, v, w	velocity components (m/s)
E	dimensionless number ($fH_0^2/\mu_0 U$)	V_n	velocity of the interface in the direction of normal unit vector (m/s)
f	the gas pressure gradient in the longitudinal direction [kg/(m$^2\cdot$ s^2)]	W	rate of strain tensor
g	gravitational acceleration (m/s^2)	x, y, z	Cartesian coordinates (m)
h	dimensionless film thickness		
H	local film thickness (m)	**Greek Symbols**	
H_c	channel height (m)	α	plate inclination angle (°)
I	identity tensor	ε	the film aspect ratio
J	nondimensional evaporation rate	κ	thermal conductivity [W/(m $\cdot$ K)]
k_1, k_2, k_3	dimensionless coefficients	λ	latent heat of vaporization (J/kg)
K	curvature of the interface (1/m)	μ	liquid dynamic viscosity [kg/(m $\cdot$ s)]
l	characteristic scale of streamwise length (m)	θ	dimensionless temperature of the liquid
L	heater length (m)	ρ	liquid density (kg/m^3)
L	Evaporation number ($\lambda D\rho_g/\kappa[T]$)	σ	surface tension (N/m)
Ma	Marangoni number ($\sigma_T[T]H_0^2/Ul\mu_0$)	ω	ratio of the channel height to the initial film thickness
n	normal unit vector		
p	pressure (N/m^2)		
P	stress tensors	**Subscripts**	
q	heat flux density released on the heater (W/m^2)	0	initial parameters of the flow (at $T = T_0$)
Q	flow rate of the liquid per unit film width (m^2/s)	g	gas phase
R	modified diffusion Peclet number ($Dl/H_0^2 U$)	x, y, z, T, ξ	derivatives on x, y, z, T, and ξ
Re	Reynolds number ($\rho Q/\mu$)	**Superscripts**	
		1	modified velocity components

initial film thickness, etc., on the evaporation process along the gas-liquid interface along an inclined heated plate was investigated in Yan and Soong (1995). To model the detailed transport processes special attention was given to the phase equilibrium and gas-liquid interface matching conditions. More recently, the assumption that vapor is passive in a vapor-liquid system with evaporation was questioned by Ozen and Narayanan (2004). The problem of locally heated liquid film sheared by gas in a channel was studied by Gatapova and Kabov (2008). A one-dimensional one-sided model was developed to examine the problem of heat and mass transfer. Nonlinear dynamics of a vapor-liquid system with an evaporating interface was studied by Kanatani and Oron (2011). In Tiwari and Davis (2011) the dynamics and stability of a thin, viscous film of volatile liquid flowing under the influence of gravity over a nonuniformly heated

substrate has been investigated using lubrication theory. Attention is focused on the regime in which evaporation balances the flow due to gravity. In Liu and Kabov (2012) the problem of a two-layer system consisting of a horizontal liquid layer in contact with its own vapor is considered. Effects of buoyancy, thermocapillarity, evaporation, and the dynamics of the vapor phase are taken into account. The results show that both the evaporation and the interfacial shear play important roles in the stability of the system. Modeling of the convective fluid flow with evaporation in the two-layer system has been done in Goncharova et al. (2013). In Kabova et al. (2014) a joint problem in the gas and liquid phases has been solved to thoroughly understand the influence of the gas phase on film pattern; heat and mass transfer, effects of evaporation, and condensation have been taken into account as well.

Motion of evaporated liquid film is widely studied experimentally as well. Rosskamp et al. (1998) conducted experimental research of evaporating liquid wall films driven by shear force in hot turbulent air flow. The dynamics of a wave film under intensive evaporation was investigated by Pavlenko et al. (2001). The dynamics and evaporation of a thin shear-driven liquid film in a microgap channel was studied experimentally by Kabov et al. (2007, 2011). In Houshmand and Peles (2013) experimental data combined with a heat transfer analysis were used to infer the mechanisms controlling the heat transfer process in a liquid water film in a microchannel

In the present paper, we investigate the dynamics and heat transfer of evaporating locally heated thin liquid film driven by the action of the gas flow in a microgap at different gravity levels. A two-sided three-dimensional mathematical model is used. For a deformable gas-liquid interface convection heat transfer in the liquid and the gas phases as well as temperature dependence of surface tension and liquid viscosity are taken into account. One of the main goals of the present work is to supplement the experimental research. Because for the real cooling systems the low gas Reynolds number value means low power inputs are needed for the cooling. One can assume that real cooling systems may also work at gas Reynolds numbers of about 100. Experimental investigations in this range of Reynolds number values are performed but there are still not enough data due to the high complexity of such experiments.

2. PROBLEM FORMULATION

We consider a system of a thin film of incompressible viscous liquid in contact with a gas moving in a flat microgap of given height H_C, Fig. 1. On the bottom wall of the channel a local heater is located and the heater's upper edge is located at the origin of the coordinate system. The system is assumed to be unbounded in the streamwise (x) and spanwise (y) directions. The acceleration of gravity is opposite to the z direction. The free interface is assumed to be immiscible and deformable. The motions of the liquid film and gas are governed by the Navier-Stokes, continuity, and energy equations in liquid (1)–(3) and gas (4)–(6) phases, and diffusion equation (7) in the gas phase.

$$\rho\left[\mathbf{v}_t + (\mathbf{v}\cdot\nabla)\mathbf{v}\right] = -\nabla p + \rho\mathbf{g} + \mathrm{div}(\mu W), \tag{1}$$

$$\nabla\cdot\mathbf{v} = 0, \tag{2}$$

$$\rho c_p\left[T_t + (\mathbf{v}\cdot\nabla)T\right] = k\nabla^2 T, \tag{3}$$

$$\rho_g\left[\mathbf{v}_{gt} + (\mathbf{v}_g\cdot\nabla)\mathbf{v}_g\right] = -\nabla p_g + \rho_g\mathbf{g} + div(\mu_g W_g), \tag{4}$$

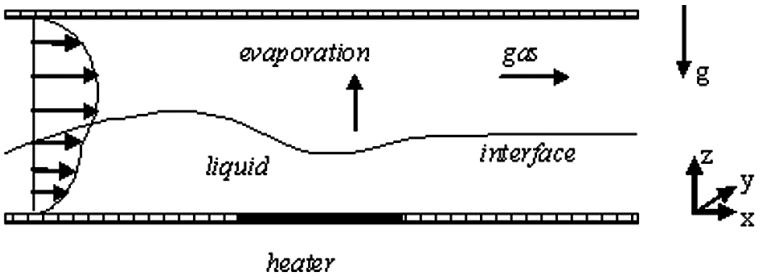

FIG. 1: A sketch of the physical model.

$$\nabla \cdot \mathbf{v}_g = 0, \tag{5}$$

$$\rho_g c_{pg} \left[T_{gt} + (v_g \cdot \nabla) T_g\right] = k_g \nabla^2 T_g, \tag{6}$$

$$C_t + (\mathbf{v}_g \cdot \nabla) C = D \nabla^2 C. \tag{7}$$

The components W_{ij} and W_{gij} $(i, j = 1, 2, 3;\ W_{ij} = W_{ji},\ W_{gij} = W_{gji})$ of rate of strain tensors W and W_g are defined as follows:

$$W_{11} = u_x, W_{g11} = u_{gx}, \quad W_{12} = (u_y + v_x)/2,\ W_{g12} = (u_{gy} + v_{gx})/2,$$

$$W_{13} = (u_z + w_x)/2, \quad W_{g13} = (u_{gz} + w_{gx})/2, \quad W_{22} = v_y, \quad W_{g22} = v_{gy}, \quad W_{g23} = (v_{gz} + w_{gy})/2,$$

$$W_{33} = w_z, \quad W_{g33} = w_{gz}.$$

We assume that the upper wall is adiabatic and impermeable:

$$\mathbf{v}_g = 0, \quad \partial T_g/\partial z = 0, \quad \partial C/\partial z = 0, \quad z = H_c, \tag{8}$$

and at the bottom wall, the no-slip condition and thermal boundary condition are satisfied:

$$\mathbf{v} = 0, \quad \kappa \partial T/\partial z = -q(t, x, y) \quad \text{or} \quad T = T_1(t, x, y), \quad z = 0. \tag{9}$$

The initial parameters such as initial film thickness, tangential stresses, the pressure drop, and velocity fields in the liquid and gas phases were found as the exact solution of the problem of isothermal laminar co-current flow in the channel with straight streamlines; for more details see the Appendix. At the initial time moment conditions (10) are assumed to be valid.

$$\begin{aligned} &H = H_0, \quad T = T_g = T_0, \quad C = C_0, \\ &u = u_0(z), \quad u_g = u_{g0}(z), \quad v = v_0(z), \quad v_g = v_{g0}(z), \quad w = w_0(z), \quad w_g = w_{g0}(z). \end{aligned} \tag{10}$$

Here the value of the initial vapor concentration C_0 should be prescribed.

At the free gas-liquid interface the condition of continuity of the tangential component of the velocity vector (no-slip condition of two viscous media) is

$$\mathbf{v} - \mathbf{n}(\mathbf{v} \cdot \mathbf{n}) = \mathbf{v}_g - \mathbf{n}(\mathbf{v}_g \cdot \mathbf{n}). \tag{11}$$

The mass conservation for the liquid media and mutual mass conservation conditions are

$$\begin{aligned} &\rho(\mathbf{v} \cdot \mathbf{n} - V_n) = \rho_g(v_g \cdot \mathbf{n} - V_n), \\ &(1 - C)\rho_g(\mathbf{v}_g \cdot \mathbf{n} - V_n) = -D\mathbf{n} \cdot \rho_g \nabla(C). \end{aligned} \tag{12}$$

The dynamic condition with the term expressing the mechanical effect of the evaporated matter on the liquid is

$$(P - P_g) \cdot \mathbf{n} = 2\sigma K \mathbf{n} + \nabla_\Gamma \sigma + \rho_g (\mathbf{v}_g \cdot \mathbf{n} - V_n)^2 (\rho_g/\rho - 1)\mathbf{n}. \tag{13}$$

Here $P = -pI + 2\mu W$, $P_g = -p_g I + 2\mu_g W_g$. The thermal boundary condition, taking into account the energy spending on the phase transition, is

$$\kappa \partial T/\partial \mathbf{n} - \kappa_g \partial T_g/\partial \mathbf{n} = \frac{\rho_g \lambda D}{1 - C} \cdot \frac{\partial C}{\partial \mathbf{n}}. \tag{14}$$

Here $\mathbf{n} = (-H_x, -H_y, 1)/\sqrt{I}$, $I = 1 + H_x^2 + H_y^2$, $V_n = H_t/\sqrt{I}$, $\nabla_\Gamma = \nabla - \mathbf{n}(\mathbf{n} \cdot \nabla)$ is the surface gradient.

In addition, conditions of local thermodynamic equilibrium (15) are posed.

$$T = T_g, \quad C = C_*(T). \tag{15}$$

T_g on the gas-liquid interface is unknown and should be determined in the process of solving a problem.

The following dependences on temperature for the concentration, surface tension, and dynamic viscosity are assumed:

$$C_* = C_0 + C_T(T - T_0) + C_{TT}(T - T_0)^2/2, \quad \mu = (1/\mu_0 + \mu_T(T - T_0) + \mu_{TT}(T - T_0)^2/2)^{-1},$$
$$\sigma = \sigma_0 - \sigma_T(T - T_0) + \sigma_{TT}(T - T_0)^2/2$$

where C_0, C_T, C_{TT}, μ_0, μ_T, μ_{TT}, σ_0, σ_T, σ_{TT} are constants, and T_0 is the constant temperature at the initial time moment.

3. DIMENSIONLESS EQUATIONS AND PARAMETERS

Let us perform the change of variables in the liquid and gas phase as follows:

$$\xi = z/H, \quad u^1 = uH, \quad v^1 = vH, \quad w^1 = w - u\xi H_x - v\xi H_y, \tag{16}$$

$$\eta = \frac{\omega - 1}{H_C - H} z - \frac{H\omega - H_C}{H_C - H}, \quad u_g^1 = \frac{H_C - H}{\omega - 1} u_g,$$
$$v_g^1 = \frac{H_C - H}{\omega - 1} v_g, \quad w_g^1 = w_g - \frac{H_C - z}{H_C - H} H_x u_g - \frac{H_C - z}{H_C - H} H_y v_g, \tag{17}$$

where $\omega = H_C/H_0$. Then the governing equations with boundary conditions could be rewritten in the layer $\xi \in (0, 1)$, $\eta \in (1, \omega)$, $-\infty < x, y < \infty$. The continuity equations in liquid and in gas retain their form in new variables but the kinematic condition at the free interface simplifies. Below only variable ξ is used so, that at $\xi > 1$ it is identified with variable η.

In order to nondimensionalize the governing equations with boundary conditions, let us define scales for the liquid velocity and longitudinal length as follows:

$$U = \frac{\mu_0}{\rho H_0}, \quad l = \left(\frac{\sigma_0 H_0^2}{\rho U^2}\right)^{1/3}, \quad \mu_0 = \mu(T_0). \tag{18}$$

For the case of prescribed heat flux on the heater the temperature scale is defined as

$$[T] = \frac{Q_0 H_0}{\kappa S_0}. \tag{19}$$

For the case of prescribed temperature at the heater the temperature scale is defined as

$$[T] = \max_{t,x,y} [T_1(t, x, y) - T_0]. \tag{20}$$

Here Q_0/S_0 is the average heat flux at the heater, S_0 the heating area.

4. GOVERNING EQUATIONS

We employ the lubrication theory, so we assume that the characteristic film thickness and the characteristic film thickness variation are much smaller than the characteristic length scale of the film in streamwise and spanwise directions $\varepsilon = H_0/l \ll 1$. The problem is reduced to a solution of five governing equations: for the film thickness (21), gas pressure (22), temperature distribution in liquid (24) and gas (25), and vapor concentration in gas phase (26):

$$h_t + \phi\left(\nabla^2\nabla^2 h - \mathbf{A}\nabla^2 h\right) + \phi_x\left(\nabla^2 h_x - \mathbf{A}h_x + \mathbf{C}\right) + \phi_y\left(\nabla^2 h_y - \mathbf{A}h_y\right)$$
$$+ \mathbf{Ma}\left[\gamma\nabla^2\theta + \gamma_x\theta_x + \gamma_y\theta_y\right] + \delta\nabla^2 p_g + \delta_x\nabla^2 p_{gx} + \delta_y\nabla^2 p_{gy} = \frac{k_3\mathbf{R}}{1 - C}\left(\frac{\omega - 1}{\omega - h}\right) C_\xi, \tag{21}$$

$$\delta_g \nabla^2 p_g + \delta_{gx} p_{gx} + \delta_{gy} p_{gy} + \phi_g \left(\nabla^2 \nabla^2 h - \mathbf{A} \nabla^2 h\right) + \phi_{gx} \left(\nabla^2 h_x - \mathbf{A} h_x + \mathbf{C}\right)$$
$$+ \phi_{gy} \left(\nabla^2 h_y - \mathbf{A} h_y\right) + \mathbf{Ma} \left[\gamma_g \nabla^2 \theta + \gamma_{gx} \theta_x + \gamma_{gy} \theta_y\right] = \mathbf{R} \frac{k_3 - 1}{1 - C} \left(\frac{\omega - 1}{\omega - h}\right) C_\xi. \tag{22}$$

Here functions ϕ, γ, δ, ϕ_g, γ_g, δ_g, U_i, U_{gi} are specified in the following form:

$$\begin{aligned} &\phi = U_1|_{\xi=1}, \quad \gamma = U_2|_{\xi=1}, \quad \delta = U_3|_{\xi=1}, \quad \phi_g = (U_1 + U_{g1})|_{\xi=1}, \\ &\gamma_g = (U_2 + U_{g2})|_{\xi=1}, \quad \delta_g = (U_3 + U_{g3})|_{\xi=1}, \\ &U_i = \int_0^\xi \Psi_i(t, x, y, \tau) d\tau, \quad U_{gi} = \int_\xi^\omega \Psi_{gi}(t, x, y, \tau) d\tau, \quad i = 1, 2, 3, \end{aligned} \tag{23}$$

where

$$\Psi_1 = h^3 F - \frac{k_1 h^4 F_1}{\omega - h + k_1 h G_1} G, \quad \Psi_2 = -\frac{h^2 (\omega - h)}{\omega - h + k_1 h G_1}, \quad \Psi_3 = -h^3 F + \frac{h^2 \left[2 k_1 h^2 F_1 - (\omega - h)^2\right]}{2 (\omega - h + k_1 h G_1)} G,$$

$$\Psi_{g1} = -\frac{h^2 (\omega - h)^2 (\omega - \xi) F_1}{(\omega - 1)^2 (\omega - h + k_1 h G_1)}, \quad \Psi_{g2} = \frac{h (\omega - h)^2 (\omega - \xi)}{(\omega - 1)^2 (\omega - h + k_1 h G_1)} G_1,$$

$$\Psi_{g3} = \frac{(\omega - h)^2 (\omega - \xi)}{(\omega - 1)^2 k_1} \left[\frac{2 h^2 k_1 F_1 - (\omega - h)^2}{2 (\omega - h + k_1 h G_1)} + \frac{(\omega - h) [(\omega - \xi) - 2 (\omega - 1)]}{2 (\omega - 1)}\right],$$

$$G_1 = G|_{\xi=1}, \quad F_1 = F|_{\xi=1}, \quad F = \int_0^\xi \frac{1 - \tau}{\mu [\theta (t, x, y, \tau)]} d\tau, \quad G = \int_0^\xi \frac{1}{\mu [\theta (t, x, y, \tau)]} d\tau,$$

$$\begin{aligned} &hD (h\theta_t - h_t \xi \theta_\xi + u\theta_x + v\theta_y + w\theta_z) = \varepsilon^2 h^2 (\theta_{xx} + \theta_{yy}) + \left[1 + \varepsilon^2 \xi^2 \left(h_x^2 + h_y^2\right)\right] \theta_{\xi\xi} \\ &- 2\varepsilon^2 h (h_x \theta_{x\xi} + h_y \theta_{y\xi}) \xi + 2\varepsilon^2 \xi^2 \left(h_x^2 + h_y^2\right) \theta_\xi - \varepsilon^2 \xi h (h_{xx} + h_{yy}) \theta_\xi, \end{aligned} \tag{24}$$

$$\begin{aligned} &\left(\frac{\omega - h}{\omega - 1}\right) D_g \left[\left(\frac{\omega - h}{\omega - 1}\right) \theta_{gt} - h_t \left(\frac{\omega - \xi}{\omega - 1}\right) \theta_{g\xi} + u_g \theta_{gx} + v_g \theta_{gy} + w_g \theta_{g\xi}\right] \\ &= \varepsilon^2 \left(\frac{\omega - h}{\omega - 1}\right)^2 (\theta_{gxx} + \theta_{gyy}) + \left[1 + \varepsilon^2 \left(\frac{\omega - \xi}{\omega - 1}\right)^2 \left(h_x^2 + h_y^2\right)\right] \theta_{g\xi\xi} \\ &- 2\varepsilon^2 \left(\frac{\omega - \xi}{\omega - 1}\right) (h_x \theta_{gx\xi} + h_y \theta_{gy\xi}) + \frac{2\varepsilon^2}{\omega - 1} \left(\frac{\omega - \xi}{\omega - 1}\right) \left(h_x^2 + h_y^2\right) \theta_{g\xi} \\ &- \varepsilon^2 \left(\frac{\omega - \xi}{\omega - 1}\right) (h_{xx} + h_{yy}) \theta_{g\xi}, \end{aligned} \tag{25}$$

$$\begin{aligned} &\left(\frac{\omega - h}{\omega - 1}\right) S_g \left[\left(\frac{\omega - h}{\omega - 1}\right) C_t - h_t \left(\frac{\omega - \xi}{\omega - 1}\right) C_\xi + u_g C_x + v_g C_y + w_g C_\xi\right] \\ &= \varepsilon^2 \left(\frac{\omega - h}{\omega - 1}\right)^2 (C_{xx} + C_{yy}) + \left[1 + \varepsilon^2 \left(\frac{\omega - \xi}{\omega - 1}\right)^2 \left(h_x^2 + h_y^2\right)\right] C_{\xi\xi} \\ &- 2\varepsilon^2 \left(\frac{\omega - \xi}{\omega - 1}\right) (h_x C_{x\xi} + h_y C_{y\xi}) - \frac{2\varepsilon^2}{\omega - 1} \left(\frac{\omega - \xi}{\omega - 1}\right) \left(h_x^2 + h_y^2\right) C_\xi \\ &- \varepsilon^2 \left(\frac{\omega - \xi}{\omega - 1}\right) (h_{xx} + h_{yy}) C_\xi. \end{aligned} \tag{26}$$

Both convective and conductive terms in the energy equations are taken into account.

The following dimensionless criteria of similarity and coefficients k_1, k_2, and k_3 are used:

$$\mathbf{A} = \frac{g\cos\alpha H_0^2}{U^2 l}, \quad \mathbf{C} = \frac{g\sin\alpha H_0}{U^2}, \quad \mathbf{Ma} = \frac{\sigma_T[T]H_0}{\mu_0 U l}, \quad \mathbf{L} = \frac{\lambda D\rho_g}{\kappa[T]},$$
$$\mathbf{S}_g = \frac{\mu_{0g}H_0}{D\rho_g}, \quad \mathbf{E} = \frac{fH_0^2}{\mu_0 U}, \quad \mathbf{R} = \frac{Dl}{H_0^2 U}, \quad \mathbf{D} = \frac{c_p\mu_0 H_0}{l\kappa}, \tag{27}$$
$$\mathbf{D}_g = \frac{c_{pg}\mu_{0g}H_0}{\kappa_g}, \quad k_1 = \frac{\mu_{0g}}{\mu_0}, \quad k_2 = \frac{\kappa_g}{\kappa}, \quad k_3 = \frac{\rho_g}{\rho}.$$

Dimensionless numbers **A** and **C** determine the values of the hydrostatical longitudinal and transverse components of the pressure gradient; the Marangoni number **Ma** specifies the thermocapillary forces on the surface of the nonuniformly heated liquid film. Evaporation number **L** characterizes the thermal loss at evaporation, number **R** characterizes mass loss at evaporation, and number **E** represents the action of the longitudinal pressure gradient. **D** and $\mathbf{D}_g$ numbers characterize the ratios of conductive and convective heat fluxes in liquid and gas phases. $\mathbf{S}_g$ is a modified Schmidt number.

Components of the velocities in liquid and gas could be calculated from the explicit formulas.

For the governing equations (24), (25), (26) and (21), (22) the additional boundary conditions should be posed. Let us assume that far from the heating area at $y \to \pm\infty, x \to -\infty$ all disturbances decay and the film surface becomes even. At $x \to +\infty$ motion remains unknown, but all changes are slow so "soft" boundary conditions could be posed. Therefore the additional boundary conditions could be expressed as follows:

$$\begin{aligned} &y \to \pm\infty, \quad x \to -\infty: \quad \theta, \theta_g \to 0; \quad h, C \to 1, \\ &x \to +\infty: \qquad\qquad \partial\theta/\partial x, \quad \partial\theta_g/\partial x, \quad \partial C/\partial x, \quad \partial h/\partial x \to 0. \end{aligned} \tag{28}$$

5. NUMERICAL METHOD

Material constants in all calculations correspond to water and nitrogen, and the inclination angle is equal to 0° (Kikoin, 1976; Nikolskii, 1966). All material constants are listed in Table 1.

The heat flux in the vicinity of the heater edges has smoothed using sine-type heat flux distribution. The smoothing has been performed to avoid temperature jumps when posing the boundary conditions, bearing in mind the fact that in experiments the heating intensity on the edges is always smoothed.

Numerical solution of the problem is implemented by the finite difference method using the grid approximation. The solution of the problem in the unlimited x, y area is changed by solution in the field $-x_1 < x < x_2$, $-y_1 < y < y_2$, $0 < \xi < \omega$. In that case the initial conditions and conditions of the heat balance remain in their form. It is assumed that the heater front edge on the substrate is located in the origin of the coordinates, and the values of x_1, x_2, y_1, y_2 are large enough so that at the borders of the computational domain, $x = -x_1$, $y = -y_1$, $y = y_2$, all disturbances decay; see (28). A flow chart of the numerical algorithm is as follows: on the first time layer the values of each grid function are known from the initial conditions. Then on each time step the calculation of the temperature is carried out. After calculation of the concentration and film thickness the calculation of the gas pressure is carried out. The alternating directions implicit (ADI) method is used to solve the system of grid equations with boundary conditions. To solve the problem on each frictional grid step the Thomas algorithm is used (Samarskii, 1971; Douglas, 1962; Peaceman and Rachford, 1955). For more details on the model, numerical algorithm and testing please refer to Kabova et al. (2014).

6. RESULTS AND DISCUSSION

Calculations have been performed for the constant channel height $H_C = 250$ μm. The channel has been supposed to be horizontal. The heater size is constant in all calculations and is equal to 1×1 cm^2 (length $\times$ width). The fluid is water and the gas is nitrogen. Gas is moving in the x-direction and the middle of the heater upper edge is located

TABLE 1: Physical parameters of the problem

T_0	**293**	***K***
D	0.34166×10^{-4}	m^2/s
c_p	0.4182×10^4	$J/(kg \cdot K)$
C_0	$0.1353938425 \times 10^{-1}$	
C_T	$0.8770091963 \times 10^{-3}$	K^{-1}
C_{TT}	$0.5451739304 \times 10^{-4}$	K^{-2}
p_0	9.80665×10^4	N/m^2
κ	0.5985	$W/(m \cdot K)$
λ	0.244465×10^7	J/kg
μ_0	0.999×10^{-3}	$kg/(m \cdot s)$
μ_T	0.24522×10^2	$kg/(m \cdot s \cdot K)$
μ_{TT}	0.17922	$kg/(m \cdot s \cdot K^2)$
ρ	0.99829×10^3	kg/m^3
σ_0	0.72601×10^{-1}	N/m
σ_T	0.15525×10^{-3}	$N/(m \cdot K)$
σ_{TT}	-0.43×10^{-6}	$N/(m \cdot K^2)$
c_{pg}	1.074842×10^3	$J/(kg \cdot K)$
κ_g	24.03×10^{-3}	$W/(m \cdot K)$
μ_{0g}	0.17559×10^{-4}	$kg/(m \cdot s)$
ρ_g	1.2505	kg/m^3

at the origin of the coordinate system. The initial temperature is equal to 20°C, and the initial concentration of vapor in the gas $\rho_g C_0 = 0.016931$ kg/m^3 corresponds to the partial pressure that corresponds to the saturation temperature equal to 20°C.

Calculations of the total amount of matter evaporated from the gas-liquid interface, $\mathbf{J}_{\rm total}$, and the amount of matter evaporated from the heating area, $\mathbf{J}_{\rm heater}$, have been performed using the following formulas:

$$\mathbf{J}_{\rm total} = \int\limits_{\Lambda} \frac{1}{h(x,y)} \frac{\partial C}{\partial \xi}\bigg|_{\xi=1} dxdy,$$

$$\mathbf{J}_{\rm heater} = \int\limits_{\Omega} \frac{1}{h(x,y)} \frac{\partial C}{\partial \xi}\bigg|_{\xi=1} dxdy.$$

Here Λ is the all area of calculations, and Ω is the heating area. Here **J** is a nondimensional evaporation rate, which is proportional by physical meaning to the value $(C_0 D \rho_g l^2)/H_0$ kg/s.

6.1 Evaporation

Calculations show that the gravity level has an important effect on the film evaporation. Figure 2 shows the amount of matter evaporated from the whole area of calculations and from the heating area versus time at two different values of heating intensity at zero gravity condition. Figure 3 shows the total amount of matter evaporated from the gas-liquid interface versus time at different gravity levels. One can see that evaporation is governed substantially by the heating intensity at any gravity level and relation is strongly nonlinear. Mainly evaporation takes place in the vicinity of the heater; for heat flux equal to 0.05 W/cm^2 the difference between $\mathbf{J}_{\rm total}$ and $\mathbf{J}_{\rm heater}$ is about 7% and for q = 1 W/cm^2 the difference is getting lower and is equal to about 2%; see Fig. 2. Decreasing of gas velocity leads to increasing intensity of evaporation; see Fig. 3. Increasing the gravity level considerably, up to 40%, decreases intensity of evaporation;

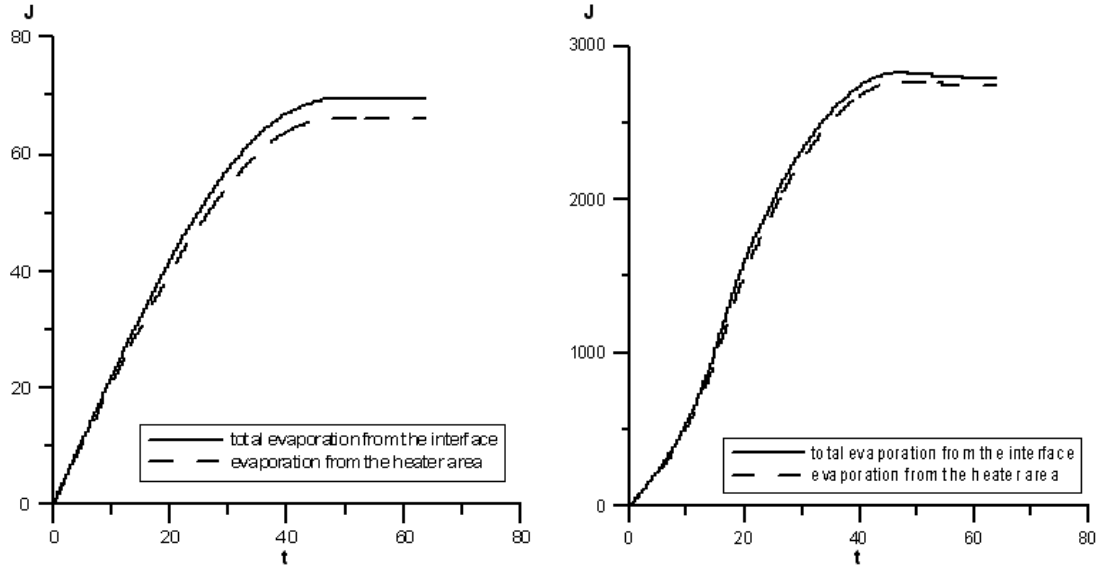

(a) (b)

FIG. 2: Total amount of matter evaporated from the gas-liquid interface versus time of the process (here and hereinafter t is a nondimensional time equal to the value tU/l [c(m/s)(1/m)]); Re $= 2$, Re$_g = 18$, $H_0 = 61.7$ μm, $0g$. (**a**) $q = 0.05$ W/cm^2, (**b**) $q = 1$ W/cm^2.

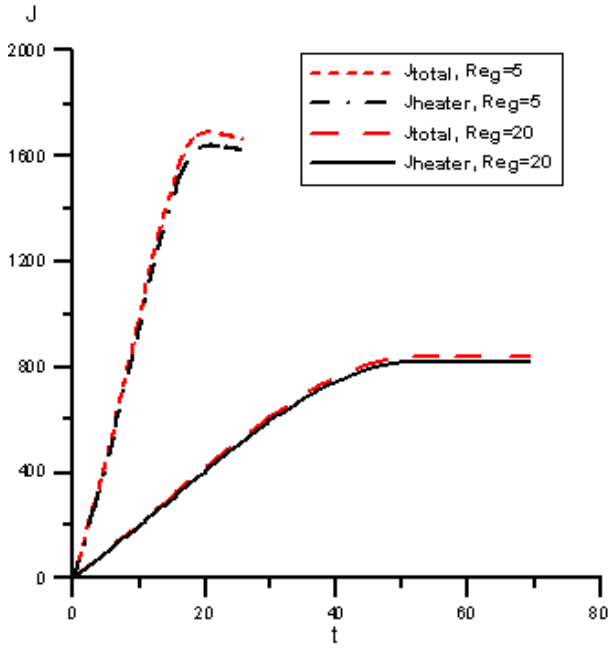

FIG. 3: Amount of matter evaporated from the gas-liquid interface, $\mathbf{J}_{\rm total}$, and from the heater, $\mathbf{J}_{\rm heater}$, versus time at different Re$_g$, $q = 0.5$ W/cm^2, Re $= 2$, $H_0 = 59.58$ μm at Re$_g = 20$ and $H_0 = 90.7$ μm at Re$_g = 5$, $20g$; here $g = 9.81$ m/s^2.

see Fig. 4. With increase of the gravity level the height of the liquid bump decreases significantly. At zero gravity the ratio of the maximum film thickness in the bump and initial film thickness is equal to 1.33 and for the normal gravity conditions this ratio is equal to 1.32. At hypergravity for $10g$ and $20g$ the parameter $H_{\max}/H_0$ is equal to 1.27 and 1.121, respectively. The minimum film thickness takes place near the end of the heater. At zero gravity the ratio of the minimum film thickness located near the end of the heater and initial film thickness is equal to 0.169 and for the normal gravity conditions this ratio is equal to 0.175. At hypergravity for $10g$ and $20g$ the parameter $H_{\max}/H_0$ is equal to 0.194 and 0.34, respectively.

As one can see, stabilization of evaporation at constant Re_g almost does not depend on the gravity level and takes place, for example, when $\mathrm{Re}_g = 20$, in 45–55 s. The time needed for stabilization of evaporation depends significantly on the gas Reynolds number; see Fig. 3. For example, between $\mathrm{Re}_g = 5$ and $\mathrm{Re}_g = 20$ it decreased by 30 s. One can see that decrease of gas velocity leads to increasing intensity of evaporation. That is rather unusual so the reason will be discussed later.

After the heater the gas-liquid interface cooldown due to evaporation and the film temperature considerably decreases; see Fig. 5. This fact has an important effect on the interface deformations and film breakdown. Notably high

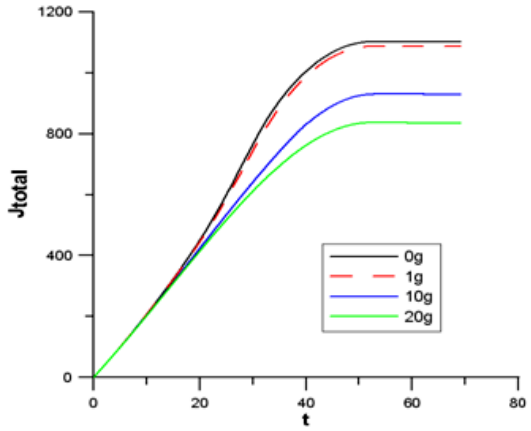

FIG. 4: Total amount of matter evaporated from the gas-liquid interface, $\mathbf{J}_{\mathrm{total}}$ versus time at different gravity levels, $q = 0.5$ W/cm^2, Re $= 2$, $\mathrm{Re}_g = 20$, $H_0 = 59.58$ μm; here $g = 9.81$ m/s^2.

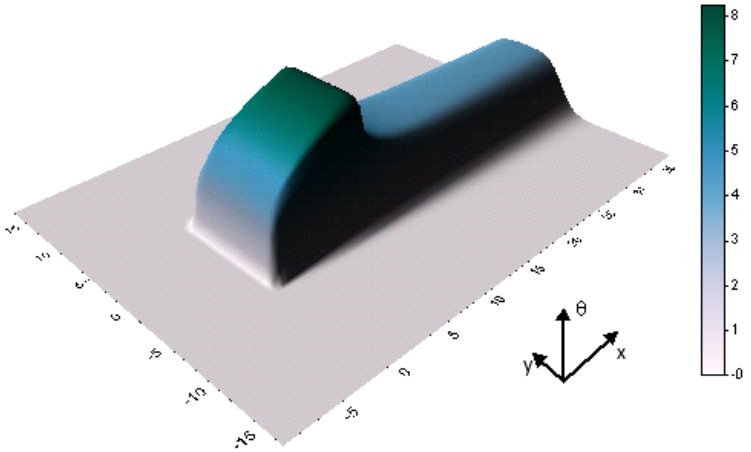

FIG. 5: Dimensionless temperature distribution at the gas-liquid interface. Dimensionless size of the heater: (0.10299E+02 × 0.10299E+02), q = 0.05 W/cm^2, Re $= 2$, $\mathrm{Re}_g = 18$, $H_0 = 61.7$ μm, $0g$.

temperature gradient directed opposite to the gas flow causes an important Marangoni effect in the vicinity of the tail part of the local heating area. This thermocapillary flow directed co-current to the gas flow and thereby provoked considerable film thinning; see Fig. 6.

6.2 Thermocapillary Deformations and Temperature Distribution

Maximum deformations of the gas-liquid interface take place for the case of zero and normal gravity. It could be seen that values of maximum and minimum film thicknesses are governed substantially by the gravity and the relation is strongly nonlinear. At hypergravity conditions the deformations become smooth and less significant; these could be the main reason for significant decreasing of evaporation intensity at hypergravity (see Fig. 4). Figure 6 shows 3D thermocapillary deformations of gas-liquid interface (view from above) for three different gravity values. It is seen that gravity significantly affects the film pattern. Two lateral waves with the length of deformation much longer than the heater length are formed near the lateral sides of the heater; for high gravity these deformations become less significant and are spread in spanwise directions. The middle stream between the two main lateral waves appears on the heater due to the capillary force; for the case of hypergravity it disappears on the distance approximately equal to the heater length; see Fig. 6. These results are in good agreement with numerical results obtained in Kabova et al. (2009) where the gravity effect on thermocapillary deformations in a film flowing under the action of co-current gas flow in a horizontal minichannel has been investigated for the case of no evaporation taken into account. It was shown that decreasing the gravity level leads to a flow destabilization; particularly, a middle stream between two main lateral waves exists at the low gravity conditions. Figures 6 and 7 show that film thickness achieves a minimum value near the sides of the heater. With decreasing of gravity level, deformations become much higher, up to 20%, and the maximum is achieved at $0g$ level. For normal and microgravity conditions the film pattern destabilizes and the second-order deformations appear outside of the main lateral waves; see Fig. 7.

From Figs. 7 and 8 one can see that even at quite low heating intensities transversal deformations in the heating area become significant (Fig. 7) and longitudinal deformation (Fig. 8) of the gas-liquid interface could be much smaller in comparison with them. The longitudinal deformations depend significantly on the value of the gas Reynolds number. For example, for the minimum film thickness, at $0g$ or $1g$ transversal deformations could come up to 40% from the initial film thickness (Fig. 7) when longitudinal deformations could not be higher than $10-20\%$ from the initial film thickness for low gas velocities (here $\mathrm{Re}_g = 20$). As is shown, increasing the gas Reynolds number leads to decreasing of the film deformations. It should be noted that for falling films longitudinal and transversal deformations caused by thermocapillary forces acting in longitudinal and transversal directions are of the same order (Frank and Kabov, 2006).

Figure 9 shows dimensionless temperature and gas-liquid interface profiles along the channel on the axis of symmetry at $y = 0$ for different gravity levels. All other parameters have been kept constant. There are three mechanisms of thermal transport: forced convection, thermal conduction, and diffusion of the hot vapor in the gas phase. Due to

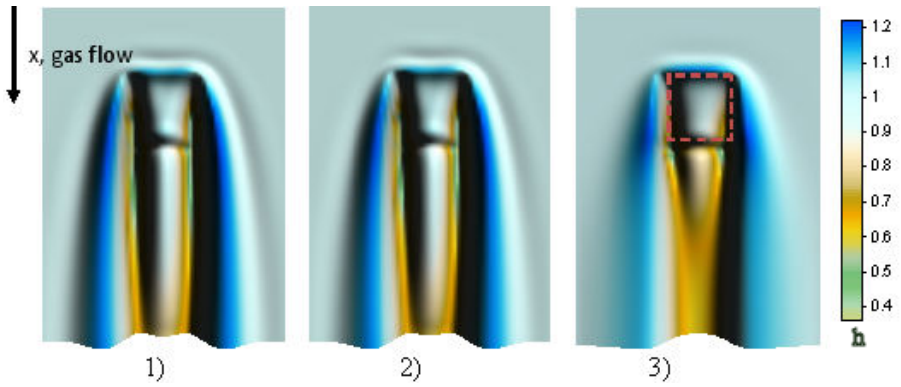

FIG. 6: Thermocapillary deformations of the gas-liquid interface (view from above), (1) $0g$; (2) $1g$; (3) $20g$. $q = 0.5$ W/cm^2, Re $= 2$, $\mathrm{Re}_g = 20$, $H_0 = 59.58$ μm, $g = 9.81$ m/s^2.

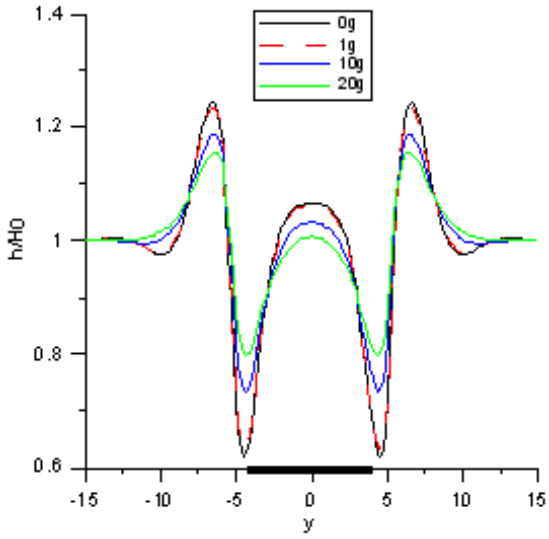

FIG. 7: Gas-liquid interface position across the channel on the heater at $x = 0.3$ cm, $q = 0.5$ W/cm^2, Re $= 2$, Re$_g = 20$, $H_0 = 59.58$ μm.

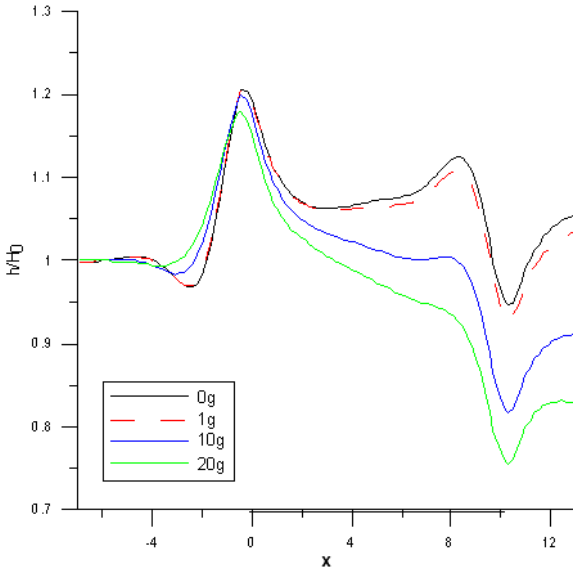

FIG. 8: Gas-liquid interface position along the channel at $y = 0$, $q = 0.5$ W/cm^2, Re $= 2$, Re$_g = 20$, $H_0 = 59.58$ μm.

the effect of thermal conductivity in the liquid, the thermal disturbances move significantly upward of the heater for all values of gravity. Because of intensive diffusion and thermal conductivity, the thermal boundary layer touches the upper wall almost at the beginning of the heater; see also Kabova et al. (2014). The position of the maximum of temperature is located near the lower boundary of the heater, then temperature stabilizes across the channel on a certain distance after the heater. For hypergravity the stabilization distance is longer.

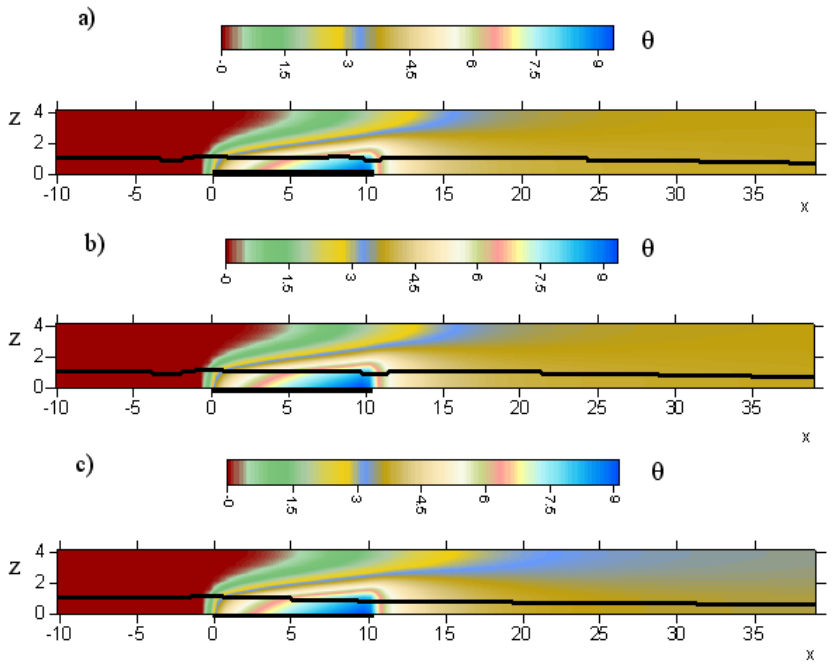

FIG. 9: Dimensionless temperature θ distribution and gas-liquid interface profiles along the channel on the axis of symmetry at $y = 0$, with color scale for temperature. (**a**) $0g$; (**b**) $1g$; (**c**) $20g$. $q = 0.5$ W/cm^2, [T] $= 0.497°$C, Re $= 2$, $H_0 = 59.58$ μm, Re$_g = 20$, $g = 9.81$ m/s^2.

6.3 Effect of the Gas Speed

From Figs. 10 and 11 one can see that for evaporation into the saturated gas, increasing the gas speed decreases the evaporation rate at any gravity level. This fact could be explained as follows: heat is needed for evaporation, but in

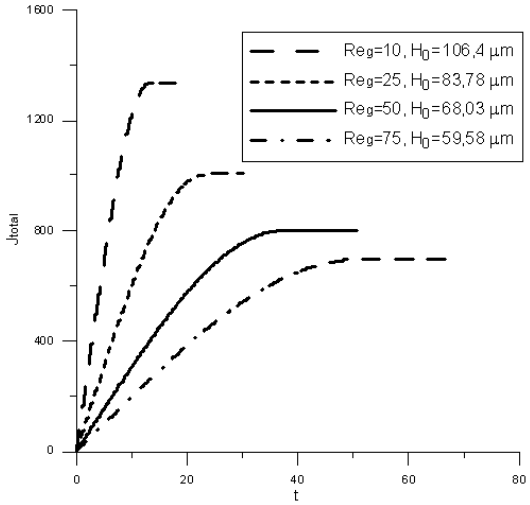

FIG. 10: Total amount of matter evaporated from the gas-liquid interface $\mathbf{J}_{\text{total}}$, at different values of gas Reynolds number Re$_g$. $q = 0.5$ W/cm^2, Re $= 5$, $20g$ where $g = 9.81$ m/s^2.

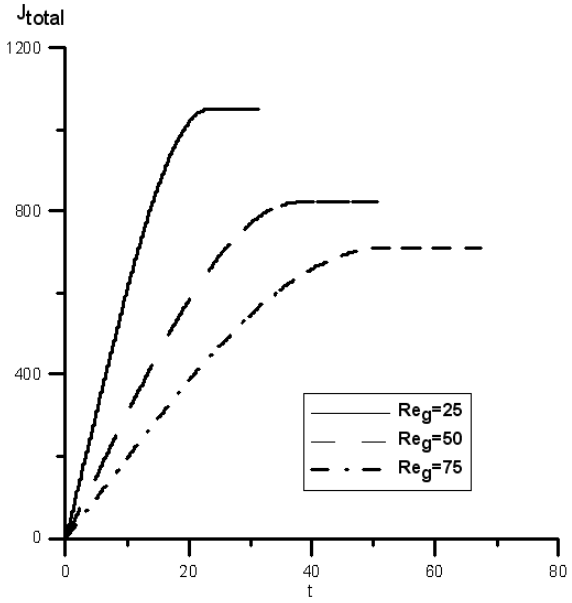

FIG. 11: Total amount of matter evaporated from the gas-liquid interface $\mathbf{J}_{\mathrm{total}}$, at different values of gas Reynolds number Re_g. $q = 0.5$ W/cm^2, Re $= 5, 0g$ where $g = 9.81$ m/s^2.

the case of intensive forced convection, heat is transported to the gas phase; as a result gas gets hot, but there is not enough heat for evaporation. This supposition could be confirmed by the fact that the situation changes to the complete opposite, if the same calculations are done for the case of constant temperature given at the heater surface; see Fig. 12. At relatively high gas speed an important part of the heat released on the heating element is transferred to the gas phase by convection which significantly affects the evaporation process as well. It is important that the initial film thickness H_0 decreases significantly with an increase of Re_g; this leads to decreasing of the liquid layer resistance and more heat comes to the liquid flow from the heater; see Fig. 12. One can see that film thickness decreases almost twice when the gas Reynolds number increases from 10 to 100.

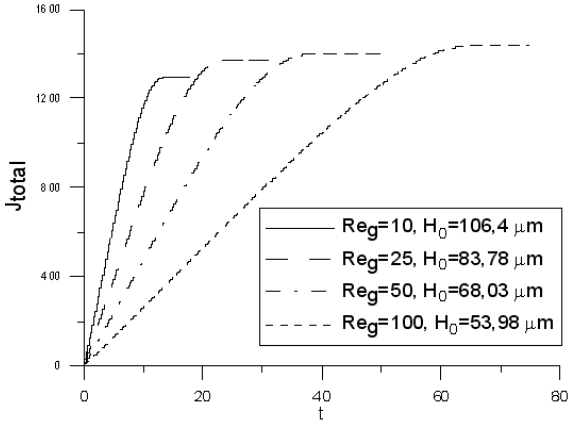

FIG. 12: Total amount of matter evaporated from the gas-liquid interface $\mathbf{J}_{\mathrm{total}}$, at different values of gas Reynolds number Re_g. Temperature at the heater surface $T = 25^{\circ}$C, Re $= 7.5, 20g$.

For the case of a given heat flux on the heater at the increasing of Re_g from 10 to 50 $\mathbf{J}_{\mathrm{total}}$ changes up to 60% but for the case of a given temperature for the same changes of the Re_g changes in $\mathbf{J}_{\mathrm{total}}$ will be about 10%; see Figs. 10, 12. At $\mathrm{Re}_g = 100$ the stabilization time of the evaporation process increases up to 60–65 s; see Fig. 12. Comparison of Figs. 11 and 12 shows that thermal boundary conditions at the wall, $q =$ constant or $T_w =$ constant, do not significantly affect the stabilization time of the evaporation process. Gravity dumps the deformations on the gas-liquid interface, so the maximum intensity of evaporation takes place at zero gravity and the minimum evaporation rate is found at higher gravity, $20g$.

7. CONCLUSIONS

Dynamics and heat transfer of evaporating locally heated thin liquid film driven by the action of the gas flow in a horizontal microgap at different gravity levels have been investigated numerically. A two-sided three-dimensional mathematical model developed in Kabova et al. (2014) has been used. For a deformable gas-liquid interface, convection heat transfer in the liquid and the gas phases as well as temperature dependence of surface tension and liquid viscosity have been taken into account. In the present paper, the influences of gravity force, the gas flow rate, heating intensity, and thermal boundary condition at the wall on the evaporation rate and gas-liquid interface deformations have been investigated for water and nitrogen; channel height and heater size have been assumed to be equal to 250 μm and 1×1 cm^2 (length $\times$ width), correspondingly. It is assumed that gravity force acts perpendicularly to the flow. In calculations the gravity level has been changed from zero gravity to hypergravity when acceleration of gravity is assumed to be up to 20 times bigger than normal Earth acceleration of gravity.

Numerically it is found that gravity significantly affects the film pattern and deformations and the effect is strongly nonlinear. Even at quite low heating intensities transversal deformations in the heating area become significant and longitudinal deformations of the gas-liquid interface could be much smaller in comparison with them. The longitudinal deformations depend significantly from the value of the gas Reynolds number. The qualitatively different effect of gas velocity on the evaporation rate is found, depending on the thermal boundary conditions on the wall, notably a given heat flux or a given temperature on the heater. For the case of a given heat intensity at the heater, increasing Re_g leads to decreasing the total amount of matter evaporated from the gas-liquid interface and for the case of a given constant temperature at the heater, increasing Re_g leads to an increase of the total amount of matter evaporated from the gas-liquid interface. Evaporation is governed substantially by the heating intensity at any gravity level and the relation is strongly nonlinear. Mainly evaporation takes place in the vicinity of the heater.

Investigations performed in the paper could be used in developing new cooling systems for microelectronics based on evaporation, and for the basic understanding of the physics of liquids under microgravity and variable gravity conditions.

ACKNOWLEDGMENTS

The study was supported by the Ministry of Education and Science of Russia (Proposal 2014-14-576-0053-069). Yu. K. gratefully acknowledges support of this work by the Russian Foundation for Basic Research (Project No14-08-31677) and by the grant of the President of the Russian Federation (Project No. K-3528.2013.8). OK gratefully acknowledge support of this work by the program to improve the competitiveness of the National Research Tomsk Polytechnic University.

REFERENCES

Bar-Cohen, A., Sherwood, G., Hodes, M., and Solbreken, G., Gas-assisted evaporative cooling of high density electronic modules, *IEEE Trans. Compon., Packag., Manuf. Technol., Part A*, vol. **18**, no. 3, pp. 502–509, 1995.

Bar-Cohen, A., Sheehan, J. R., and Rahim, E., Two-phase thermal transport in microgap channels—Theory, experimental results, and predictive relations, *Microgravity Sci. Technol.*, vol. **24**, no. 1, pp. 1–15, 2012.

Celata, G. P., Colin, C., Colinet, P., Di Marco, P., Gambaryan-Roisman, T., Kabov, O., Kyriopoulos, O., Stephan, P., Tadrist, L., and Tropea, C., Bubbles, drops, films: Transferring heat in space, *Europhys. News*, vol. **39**, pp. 23–25, 2008.

Chandra, V. and Savery, C. W., Forced convection heat and mass transfer from a falling film to a laminar external boundary layer, *Int. J. Heat Mass Transfer*, vol. **17**, pp. 1549–1557, 1974.

Chow, L. C. and Chung, J. N., Evaporation of water into a laminar stream of air and superheated stream, *Int. J. Heat Mass Transfer*, vol. **26**, pp. 373–380, 1983.

Douglas, J., Alternating direction methods for three space variables, *Numer. Math*., vol. **4**, pp. 41–63, 1962.

Frank, A. M., and Kabov, O. A., Thermocapillary structure formation in a falling film: Experiment and calculations, *Phys. Fluids*, vol. **18**, no. 3, p. 032107, 2006.

Gatapova, E. Ya. and Kabov, O. A., Shear-driven flows of locally heated liquid films, *Int. J Heat Mass Transfer*, vol. **51**, no. 19-20, pp. 4797–4810, 2008.

Goncharova, O. N., Hennenberg, M., Rezanova, E. V., Kabov, O., A, Modeling of the convective fluid flows with evaporation in the two-layer system, *Interfacial Phenomena Heat Transfer*, vol. **3**, DOI: 10.1615/InterfacPhenomHeatTransfer.2013007483, 2013.

Houshmand, F. and Peles, Y., Convective heat transfer to shear-driven liquid film flow in a microchannel, *Int. J Heat Mass Transfer*, vol. **64**, pp. 42–52, 2013.

Kabov, O. A., Lyulin, Yu. V., Marchuk, I. V., and Zaitsev, D. V., Locally heated shear-driven liquid films in microchannels and minichannels, *Int. J. Heat Fluid Flow*, vol. **28**, pp. 103–112, 2007.

Kabov, O. A., Zaitsev, D. V., Cheverda, V. V., and Bar-Cohen, A., Evaporation and flow dynamics of thin, shear-driven liquid films in microgap channels, *Exp Therm Fluid Sci*, vol. **35**, no. 5, pp. 825–831, 2011.

Kabova, Y. O., Kuznetsov, V. V., and Kabov, O. A., The effect of gravity and shear stress on a liquid film driven in a horizontal minichannel at local heating, *Microgravity Sci. Technol*., vol. **21**, no. 1, pp. 145–152, 2009.

Kabova, Yu., Kuznetsov, V. V., Kabov, O., Gambaryan-Roisman ,T., and Stephan, P., Evaporation of a thin viscous liquid film sheared by gas in a microchannel, *Int. J Heat Mass Transfer*, vol. **68**, pp. 527–541, 2014.

Kanatani, K. and Oron, A., Nonlinear dynamics of confined thin liquid-vapor bilayer systems with phase change, *Phys. Fluids*, vol. **23**, no. 3, p. 032102, 2011.

Kikoin, I. K., Ed., *Tables of Physical Units*, Handbook. Moscow: Atomizdat, 1976.

Liu, R. and Kabov, O. A., Instabilities in a horizontal liquid layer in concurrent gas flow with an evaporating interface, *Phys. Rev. E*, vol. **85**, pp. 066305-1–066305-10, 2012.

Nikolskii, V. P. Ed., *Chemist Directory*, 2nd ed., vol. 1, Corr.-member of RAS. Moscow: Chemistry, 1966.

Ozen, O. and Narayanan, R., The physics of evaporative and convective instabilities in bilayer systems: Linear theory, *Phys. Fluids*, vol. **16**, no. 12, pp. 4644–4652, 2004.

Pavlenko, A. N., Lel', V. V., Serov, A. F., and Nazarov, A. D., Flow dynamics of an intensively evaporating wave film of a liquid, *J. Appl. Mech. Tech. Phys*., vol. **42**, no. 3, pp. 475–481, 2001.

Peaceman D. and Rachford H., The numerical solution of parabolic and elliptic differential equations, *J. Indust. Math. Soc*., vol. **3**, no. 1, pp. 28–41, 1955.

Rosskamp, H., Willmann, M., and Witting, S., Heat up and evaporation of shear driven liquid films in hot turbulent air flow, *Int. J. Heat Fluid Flow*, vol. **19**, pp. 167–172, 1998.

Samarskii, A. A., *Introduction to the Theory of Difference Schemes*, Moscow: Nauka, (in Russian), 1971.

Schroppel, J. and Thiele, F., On the calculation of momentum, heat and mass transfer in laminar and turbulent flow along a vaporizing liquid film, *Numer. Heat Transfer*, vol. **6**, pp. 475–496, 1983.

Spindler, B., Linear stability of liquid film with interfacial phase change, *Int. J. Heat Mass Transfer*, vol. **25**, no. 2, pp. 161–173, 1981.

Squires T. M. and Quake S. R., Microfluidics: fluid physics at the nanoliter scale, *Rev. Mod. Phys.*, vol. **77**, pp. 977–1026, 2005.

Tiwari, N. and Davis, J. M., Stability of a volatile liquid film spreading along a heterogeneously-heated substrate, *J Colloid Interface Sci.*, vol. **355**, pp. 243–251, 2011.

Yan, W. M., Effect of film evaporation on laminar mixed convection heat and mass transfer in a vertical channel, *Int. J. Heat Mass Transfer*, vol. **35**, pp. 3419–3429, 1992.

Yan, W. M. and Soong, C. Y., Convective heat and mass transfer along an inclined heated plate with film evaporation, *Int. J. Heat Mass Transfer*, vol. **38**, no. 7, pp. 1261–1269, 1995.

APPENDIX

The initial parameters such as initial film thickness, tangential stresses, the pressure drop, and velocity fields in the liquid and gas phases were found as the exact solution of the problem of isothermal laminar co-current flow in the channel with straight streamlines. Notably the time-dependent problem of joint gas and liquid film flow in a minichannel is considered. The transport processes in liquid film and in gas are described by the Navier-Stokes and continuity equations.

In the liquid phase, at $z < H_0$:

$$\rho\left[\vec{\mathbf{v}}\cdot\nabla\vec{\mathbf{v}}\right] = -\nabla p + \rho\tilde{\mathbf{g}} + \mu\nabla^2\vec{\mathbf{v}}, \tag{A1}$$

$$\nabla\cdot\vec{\mathbf{v}} = 0, \tag{A2}$$

and in the gas phase, at $H_0 < z < d$:

$$\rho_g\left[\vec{\mathbf{v}}_g\cdot\nabla\vec{\mathbf{v}}\right] = -\nabla p_g + \rho_g\tilde{\mathbf{g}} + \mu_g\nabla^2\vec{\mathbf{v}}_g, \tag{A3}$$

$$\nabla\cdot\vec{\mathbf{v}}_g = 0, \tag{A4}$$

with boundary conditions:

$$\vec{\mathbf{v}}|_{z=0} = 0, \quad \vec{\mathbf{v}}|_{z=H_0} = \vec{\mathbf{v}}_g|_{z=H_0}, \quad \vec{\mathbf{v}}_g|_{z=d} = 0, \tag{A5}$$

and stress continuity condition at $z = H_0$:

$$(P - P_g)\cdot\vec{\mathbf{n}} = 2\sigma K\vec{\mathbf{n}}. \tag{A6}$$

Here $\vec{\mathbf{v}}$, $\vec{\mathbf{v}}_g$ are velocity vectors in the liquid and gas phases, p and p_g are pressure in the liquid and gas, ρ is liquid density, α is the inclination angle, and $\mathbf{n} = (0,0,1)$ is the normal vector.

Such problem can be solved exactly; notably we are looking for a solution in the following form:

$$\vec{\mathbf{v}} = (u,0,0), \quad \vec{\mathbf{v}}_g = (u_g,0,0), \quad u = u(z), \quad u_g = u_g(z). \tag{A7}$$

Normally $\rho_g \ll \rho$; therefore in the gas phase the effect of gravity could be neglected and motion is caused by the longitudinal pressure gradient $\nabla p_g = (-f, 0, 0)$, where f is the given pressure drop, proportional to Re_g.

So pressure in the gas could be determined as $p_g = p_0 - fx$, $p_0 = \text{const}$, $f = \text{const}$ (36) and the liquid pressure would be equal to

$$p = p_0 - fx - \rho g z\cos\alpha. \tag{A8}$$

So the problem (29)–(32) could be reduced to the solution of two equations:
In the liquid,

$$u_{zz} = -\frac{f + \rho g\sin\alpha}{\mu}, \tag{A9}$$

and in the gas,

$$(u_g)_{zz} = -\frac{f}{\mu_g}, \tag{A10}$$

with boundary conditions (33) and condition (34) in simplified form, notably

$$\mu_g\left[u_g(H_0)\right]_z = \mu\left[u(H_0)\right]_z. \tag{A11}$$

This problem could be solved exactly. Formulas for liquid and gas velocity were determined as follows:

$$u = -A_1\frac{z^2}{2} + B_1 z,$$

$$u_g = -A_2\frac{z^2}{2} + B_2 z + C_2,$$

where constants were determined as

$$A_1 = \frac{f + \rho g \sin\alpha}{\mu}, \quad A_2 = \frac{f}{\mu_g},$$

$$B_1 = \frac{A_1\mu_g H_0^2 + A_2\mu_g(d^2 - H_0^2) + 2(A_1\mu - A_2\mu_g)H_0(d - H_0)}{2\left[\mu(d - H_0) + \mu_g H_0\right]},$$

$$B_2 = \frac{A_1\mu H_0^2 + A_2\mu(d^2 - H_0^2) - 2(A_1\mu - A_2\mu_g)H_0^2}{2\left[\mu(d - H_0) + \mu_g H_0\right]},$$

$$C_2 = A_2\frac{d^2}{2} - B_2 d.$$

Then formulas for liquid and gas flow rates will be as follows:

$$Q = -A_1\frac{H_0^3}{6} + B_1\frac{H_0^2}{2}, \quad Q_g = -A_2\frac{d^3 - H_0^3}{6} + B_2\frac{d^2 - H_0^2}{2} + C_2(d - H_0).$$

Thereafter $\mathrm{Re} = Q\rho/\mu$, $\mathrm{Re}_g = Q_g$, ρ_g/μ_g. For the case of prescribed gas and liquid Reynolds numbers initial film thickness can be calculated using these formulas.